2014

Design Of A Turgo Two-Phase Turbine Runner

Youssef Aaraj
EReIE, youssef.aaraj@ereie-sas.fr

Sorina Mortada
EReIE, sorina.mortada@ereie-sas.fr

Denis Clodic
EReIE, denis.clodic@ereie-sas.fr

Maroun Nemer
Mines Paristech, maroun.nemer@mines-paristech.fr

DESIGN OF A TURGO TWO-PHASE TURBINE RUNNER

Youssef AARAJ[1, 2], Sorina MORTADA[1], Denis CLODIC[1], Maroun NEMER[2]

[1]EReIE, Palaiseau,
Essonne, Ile de France, France
+33 1 80 38 41 41/ youssef.aaraj@ereie-sas.fr

[2]CES LAB, Mines Paristech, Palaiseau,
Essonne, Ile de France, France
+33 1 69 19 17 10/ youssef.aaraj@mines-paristech.fr

ABSTRACT

A two-phase impulse turbine used to replace the classic expansion valve in a refrigeration system needs a nozzle/expander to transform the flow stored enthalpy into kinetic energy, and a runner that comes afterwards to transform the flow kinetic energy into torque. That process transforms the isenthalpic expansion of the refrigerant into, ideally, an isentropic one. Replacing a classic isenthalpic expansion with a nearly isentropic one increases the cycle cooling capacity between 8% and 20% for the same compressor input power and generates an additional electric power by the two-phase turbine.

During the expansion in the nozzle, the static pressure of the flow decreases and a phase change occurs, for the flow is slightly subcooled, by 2 to 3 K, at the nozzle entrance. A Turgo turbine runner design is presented. The runner makes use of the kinetic energy of a two-phase flow and transforms it into torque. The geometry and material of the runner components are chosen to provide mechanical integrity and high efficiency. The design takes into consideration the number of buckets, the flow behavior inside a bucket, the power loss due to drag force, the flow impingement angle with the bucket and many other factors. The variation of the efficiency of the runner with the refrigerant quality and the gas physical properties is also studied. FEM (finite element method) is used to calculate the mechanical stress on the structure of the runner that is supposed to withstand static and fatigue stresses, and erosion due to the two-phase nature of the flow. FEM is also used to visualize the flow inside the bucket and to estimate the power loss due to drag force. The calculated efficiency of the runner would be compared in the future to the efficiency of a similar to be tested runner.

1. INTRODUCTION

A refrigeration system following the Evans thermodynamic cycle has four main components: a condenser, an evaporator, a compressor, and an expansion valve. It is possible to improve the efficiency of that cycle by recovering the lost energy in the expansion valve. An isenthalpic expansion occurs in the expansion valve: the flow is expanded, transforming part of its enthalpy into kinetic energy and then transforming it back into enthalpy, by friction. An isentropic or near isentropic expansion occurs when the kinetic energy is recovered by another device (i.e. a turbine) and transformed into work before it could be transformed back into enthalpy. A two-phase turbine can provide such expansion while being able to handle a two-phase flow. In the refrigeration cycle, the two-phase turbine is placed in parallel to the expansion valve to bypass it as in Figure 1.b. Figure 1.a shows the T-s diagram of the refrigeration cycle using an expansion valve or a turbine. The isentropic expansion allows lower vapor qualities than isenthalpic ones at the evaporator inlet. This induces higher cooling capacity for the same compressor electrical consumption. The efficiency improvement of a refrigeration cycle is important because refrigeration and air conditioning account for 15 to 23% of the global electric consumption. This consumption may increase tenfold by the year 2050 (Cox, 2010).

The two-phase turbine is composed of two main parts: the expansion device and the kinetic energy recovery device. The expansion device receives the fluid in its slightly subcooled liquid form and transforms it into a two-phase flow. The kinetic energy of the flow increases with the decrease of the flow density, which by the law of conservation of mass increases the flow velocity. That increase in velocity leads to a static pressure decrease in the flow. The kinetic energy recovery device deals with transforming the kinetic energy of the two-phase flow into useful mechanical work. This paper discusses the kinetic energy recovery device, which is chosen to be a Turgo turbine wheel. The state-of-the-art is presented first, then the design of the turbine wheel different parts is discussed. Two CAD software, Autodesk Inventor 2013 and SolidWorks 2009, are used to design and mechanically analyze the wheel. While a CFD software, Fluent13, is used to represent and analyze the two-phase flow in the wheel.

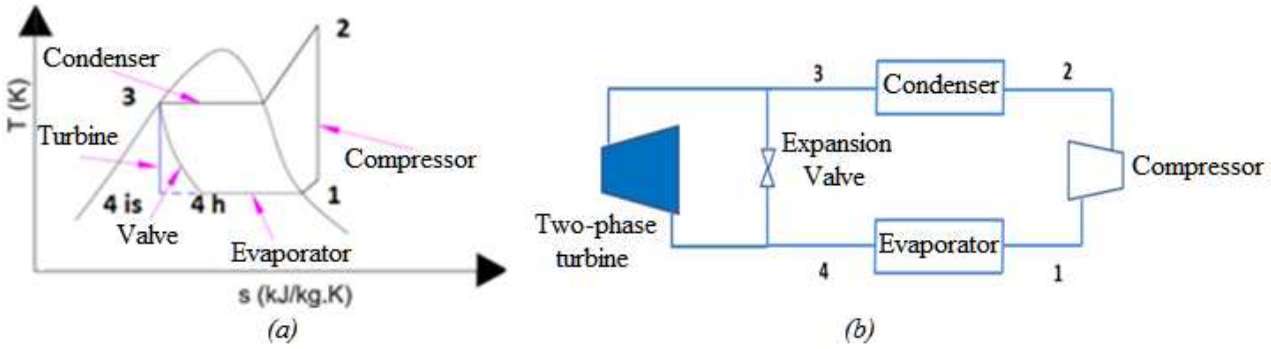

Figure 1: a) TS diagram of a refrigeration cycle with the isenthalpic expansion of an expansion valve and the isentropic expansion of a two-phase turbine, **b)** A two-phase turbine in parallel to the expansion valve.

2. STATE-OF-THE-ART

The two types of turbines that are considered to be adapted to a two-phase flow are the Hero turbine and the Turgo turbine.

2.1 Hero Turbine

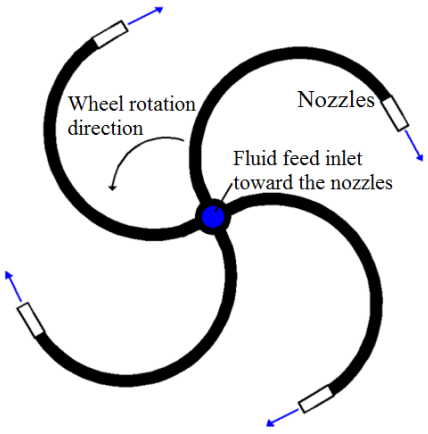

Figure 2: Hero turbine diagram.

The Hero turbine, in Figure 2, is an old reaction turbine. Its main advantage is the fact that the moment at the wheel is generated by the propulsion force. So the homogeneity of the two-phase flow and its dispersion at the nozzle exit is not an issue. Although that is a considerable advantage compared to an impulse turbine, the Hero turbine design has many flaws when used as a two-phase flow expander:

- The Hero turbine is a centrifugal turbine. The fluid is subject to a pumping effect during its expansion in the arms and nozzles of the turbine. This pumping effect may even prevent the fluid from transforming into a two-phase flow.
- The flow is pushed against the outer walls of the canals, creating more friction.

2.2 Turgo Turbine

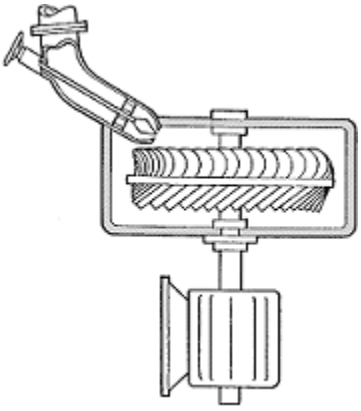

Figure 3: Sketch of a Turgo turbine (Photo credits: University of Edinburgh, School of Engineering).

The Turgo turbine, in Figure 3, is an impulse turbine. The jet coming out of the nozzle hits one or multiple buckets, rotating the turbine wheel and thus creating mechanical power. The main disadvantage of such turbine when used for two-phase flow, is the drag between the exposed areas of the buckets and the surrounding vapor/gas. The vapor density inside the turbine considered for this article is 15.5 kg/m^3, which is 13 times bigger than the density of air of 1.2 kg/m^3 at ambient temperature and pressure. Another disadvantage is the atomization and dispersion of a two-phase flow after exiting its nozzle. However, compared to the Hero turbine, the Turgo turbine has clear advantages:

- No pumping effect experienced by the fluid in the Turgo turbine
- The Turgo turbine has a simpler mechanical design
- The drag in a Turgo turbine can be low due to its small wheel diameter

Due to the counter intuitive design of a Hero turbine, when used as a two-phase turbine, and disadvantages and advantages of each turbine, the Turgo turbine design is chosen for the two-phase turbine. In addition, a horizontal wheel configuration is chosen.

3. GENERAL DIMENSIONS

For the turbine design, a two-phase mass flow rate of 4 kg/s of R-134a is considered. This flow is divided between 5 nozzles, each providing 0.8 kg/s at a vapor quality of 20%. The velocity of this flow is 60 m/s; both phases have the same velocity. The pressure inside the turbine is 3.2 bar. In order to optimize the geometry of the wheel, drag losses and kinetic energy losses due to friction inside the buckets are characterized.

3.1 Losses Inside the Bucket

A bucket profile is drawn in 2D then transformed to 3D (Figures 4.a and 4.b). The bucket has a height of 40 mm and the active surface, or the surface that is impacted by the jet, has a length of 30 mm. The profile favors the evacuation of the fluid from the bottom due to a low inflection point in its concave profile. The inflection point is situated at a distance of 27 mm from the top of the bucket. The vertical distance between the top of the bucket and the nozzle is theoretically zero to minimize the dispersion of the flow at the nozzle exit. Figure 4.c shows the position of the nozzle relatively to the bucket. The nozzle tip is tilted 20° downward and tilted with an angle of 10° towards the center of the wheel. This configuration is a result of an optimization between limiting the dispersion of the two-phase flow before hitting the bucket, and the force lost due to the angles of the jet impingement. The dispersion of similar jets is studied by Cleary *et al.* (2007) and Polanco *et al.* (2010).

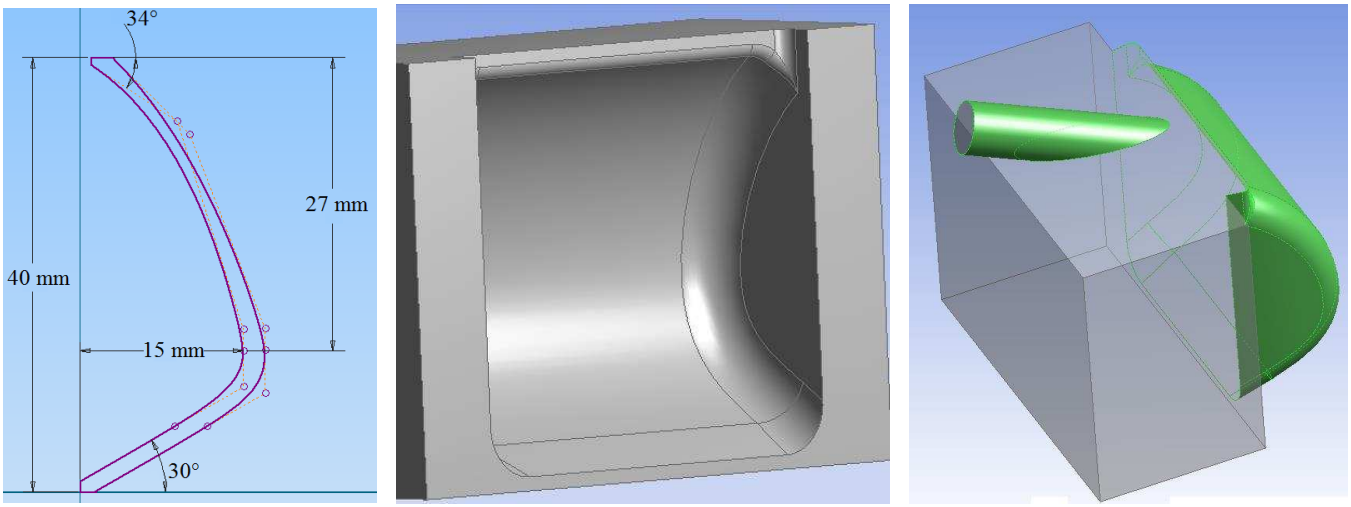

Figure 4: a) (left) Turgo turbine bucket 2D profile, **b)** (center) Turgo turbine bucket in 3D, **c)** (right) Position of the nozzle tip, the horizontal and vertical angles in the nozzle position can be clearly seen.

The jet impingement inside the bucket is simulated in the CFD software Fluent13. The simulation takes into account the bucket rotation, so the bucket active surface is rotated to simulate the rotation of the turbine wheel. For the rotation, the effective radius of the wheel, which is the distance from the wheel axis to the jet impingement point on the bucket, is considered to be 100 mm, and three adjacent buckets are simulated. The three buckets are rotated around the wheel axis for an angle of 60° at a rotational speed of 314.16rad/s, or 3000 RPM. The angle of 60° is verified geometrically to be more than enough to cover the interaction between the jet and one bucket. The simulation is chosen to be transient for a more stable solution, the K-epsilon turbulence model is chosen and the jet inlet conditions are identical to the data given at the beginning of this section. The liquid phase is at the center of jet and surrounded by the vapor phase. The jet inlet, which is the nozzle outlet, has a diameter of 15 mm and is designed as a mass flow inlet. The bucket active surface has a roughness of 10 µm, which is a typical value for aluminum after being sand cast, and the borders of the simulation space are outlets and are designated as pressure outlets, with a pressure value of 3.2 bar. After the simulation is done, the resulting velocity profile and the liquid phase distribution are given in Figures 5.a and 5.b.

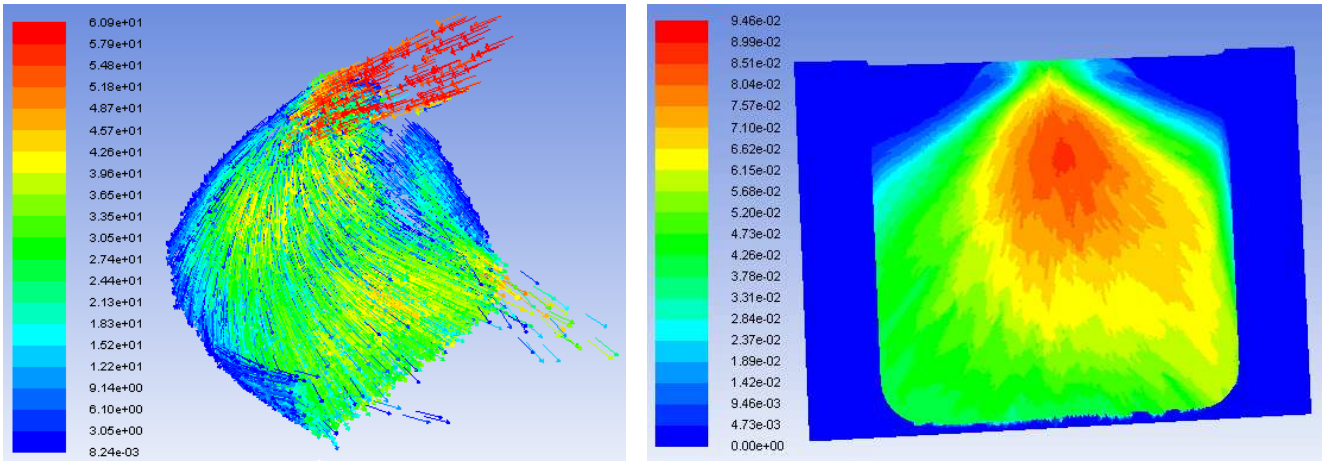

Figure 5: a) (left) Absolute velocity profile of the two-phase jet (values in m/s), **b)** (right) Liquid phase volume fraction.

Figure 5.a shows a view of the free surface flow of the two-phase jet at a time instant. The velocity at the bucket exit is lower compared to the initial jet velocity, due to friction, turbulence created inside the bucket and energy transfer to the bucket. Calculating the force exerted on the three drawn buckets active surfaces shows that the force on the buckets is equal to 83% of the theoretical force calculated by Equation (1).

$$F = 2\dot{m}v_r \quad (1)$$

Figure 5.b shows the distribution of the liquid phase on a bucket wall. The liquid phase is more concentrated at the bucket center, while the vapor phase is more concentrated on the bucket edge. For the calculation of the power transmitted from the jet to the bucket, the relative exiting velocity in the bucket would be equal to 0.8 the relative entering velocity. This result is reached after calculating the average relative tangential velocity of the flow on the outlets.

3.2 Aerodynamic Drag Losses

To characterize the aerodynamic drag losses, other CFD simulations are done. The same bucket profile as in Figure 4.a is used and is developed to a 3D bucket. The turbine wheel has 20 buckets, and since we have a periodic geometry, only one bucket is simulated while setting the radial borders of the mesh to be periodic. Figure 6.a is the full wheel, while Figure 6.b shows the simulated part.

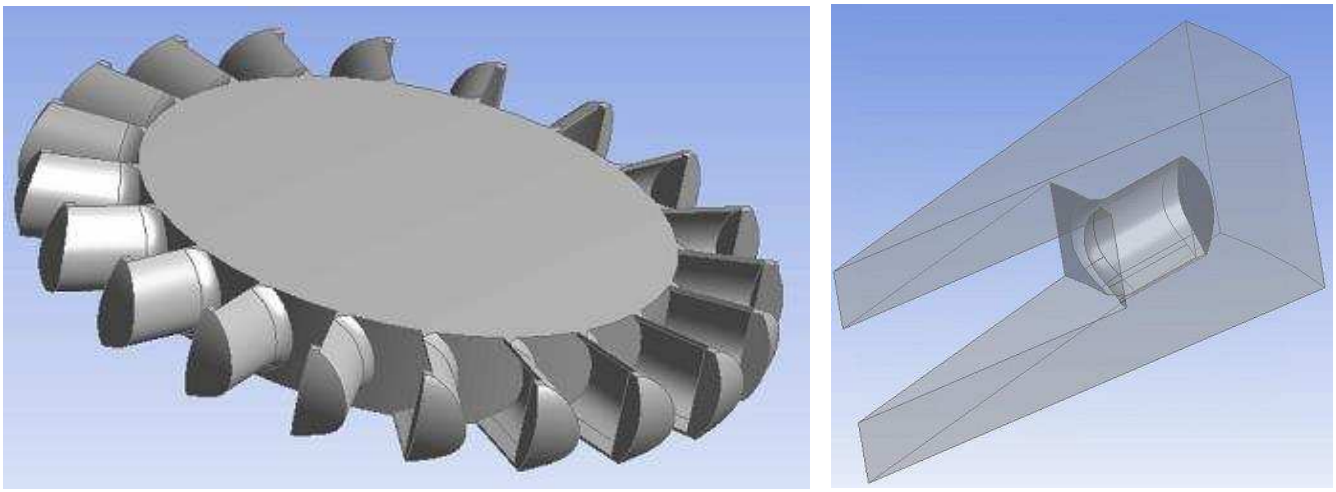

Figure 6: a) (left) The complete turbine wheel, **b)** (right) The simulated part of the turbine wheel, representing one twentieth of the complete wheel.

Multiple simulations have been done while varying the effective wheel radius between 68 and 128 mm, in steps of 5 mm. The total radius of the wheel is 22 mm larger than the effective wheel radius; this extra length is because the jet hits the bucket in its center in the radial direction, and because the bucket is 7 mm thick on the side edge. The simulation space represents the real size of the turbine enclosure. The single rotating frame method is chosen. The outside walls are fixed, the fluid domain is rotated at a speed of 3000 RPM in the direction of the wheel rotation, and the wheel is stationary relatively to the fluid domain. The simulation domain has no inlet or outlet; it is limited by the outside walls, the wheel, and the periodic boundaries. The standard K-omega turbulence model is chosen, so the mesh is refined to obtain the appropriate value of y^+ at the wheel boundary. The refrigerant R-134a properties at vapor saturation for a pressure of 3.2 bar are chosen for the fluid and an operating pressure of 3.2 bar is chosen. The simulations are performed and the power lost due to aerodynamic drag for each radius is presented in Figure 7.

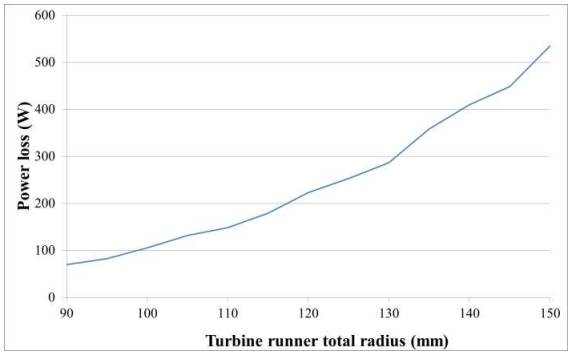

Figure 7- Power loss due to the aerodynamic drag.

The curve in Figure 7 shows a polynomial regression. Equation (2), which was developed by Diab *et al.* (2004), is used to adapt the results in Figure 7 to an equation that relies on physical properties. Equation (2) was developed to evaluate the aerodynamic drag losses caused by the gears teeth.

$$P = z\rho x b \omega^3 (R - x/2)^3 \quad (2)$$

Equation (2) resembles the classic drag power equation, but the constant drag coefficient C_D is replaced by the empirical factor z, which takes into account the turbulence created between the buckets. Another difference between Equation (2) and the classic drag power equation is x, which, in the case of the Turgo turbine runner, is the active length of the bucket in the radial direction. The active length is the part of the bucket that is not hidden from the surrounding fluid by the following bucket. From the results of the Fluent13 simulations, z is found to be equal to 0.06.

3.3 Designing the Runner

The results of the CFD calculations are used to optimize the geometry of the runner and the bucket. An iterative code is developed to determine the following things: number of buckets, effective radius (the total radius is 22 mm larger), and the top and bottom angles of the bucket as in Figure 4.a. The iterative code takes into account the following phenomena to maximize the turbine output power:

- The aerodynamic drag losses.
- The friction losses inside the bucket.
- The portion of the two-phase jet that is intercepted by the top side or "roof "of the bucket. That portion power is considered to be lost. This loss is minimized by carefully designing the back side of the bucket, so its interception of the two-phase jet is minimal.
- The mechanical friction has a fixed value of 300 W.
- The mass flow rates that exit the bucket from the top and the bottom depending on the incidence angle in the vertical plane. This incidence angle depends on the profile of the bucket. So it is a manually iterated value, after each run, the 2D bucket profile is drawn, and the average incidence angle value is put in the code.
- The mass flow rates that exit the bucket from the right side or left side of the bucket depending on the incidence angle in the horizontal plane (each of the left and right side has a different effective radius).
- The number of buckets should ensure that the two-phase jet is always in contact with at least one bucket.
- The number of buckets should ensure that the two-phase jet does not impinge the bucket lower than its inflection point (Figure 4.a).
- The exiting angles at the bucket top and bottom ensures that the exiting flow does not hit the back of the next bucket.

According to the calculation code, the best runner configuration is to have 24 buckets, an effective radius of 90 mm, which gives a total radius of 112 mm, and the buckets top and bottom angles to be equal to 35° each. The turbine mechanical power is equal to 4.5 kW, out of 11 kW available from an isentropic expansion between the condenser and the evaporator of the considered refrigeration cycle. The designed turbine has a mechanical efficiency of 40.1%. The mechanical efficiency is the mechanical power delivered by the turbine, 4.5 kW in this case, divided by the power available in an isentropic expansion, 11 kW in this case. The refrigeration power gained by the refrigeration cycle is equal to 5 kW, counting the aerodynamic drag losses and mechanical losses inside the turbine. This increase in the refrigeration power represents an increase of 0.8% of the total refrigeration power of the considered refrigeration cycle.

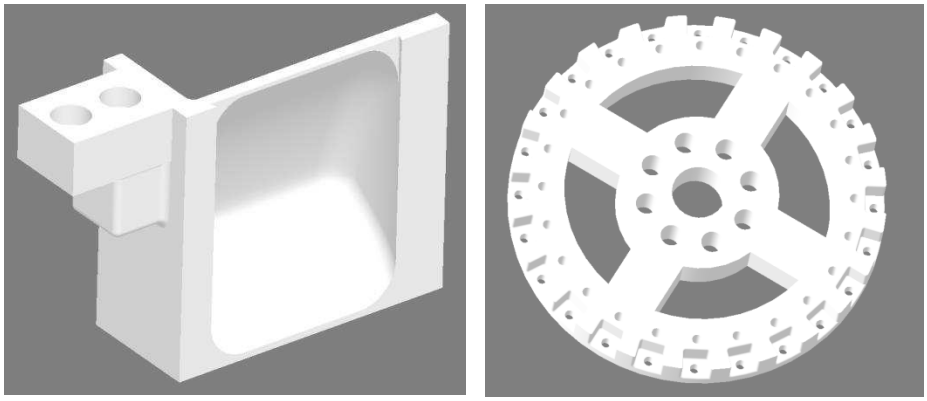

Figure 8: a) (left) 3D drawing of one bucket, **b)** (right) 3D drawing of the wheel hub.

The design results are used to draw 3D drawings of the turbine. One bucket and the wheel hub are represented in Figures 8.a and 8.b. respectively. Every turbine part is analyzed mechanically, in static stress and in fatigue stress. The resonance frequencies are also calculated to be sure to have a 15% margin between the wheel speed and the nearest critical speed, as suggested by Yun and Lin (2013). A section view of the entire turbine closure is given in Figure 9.

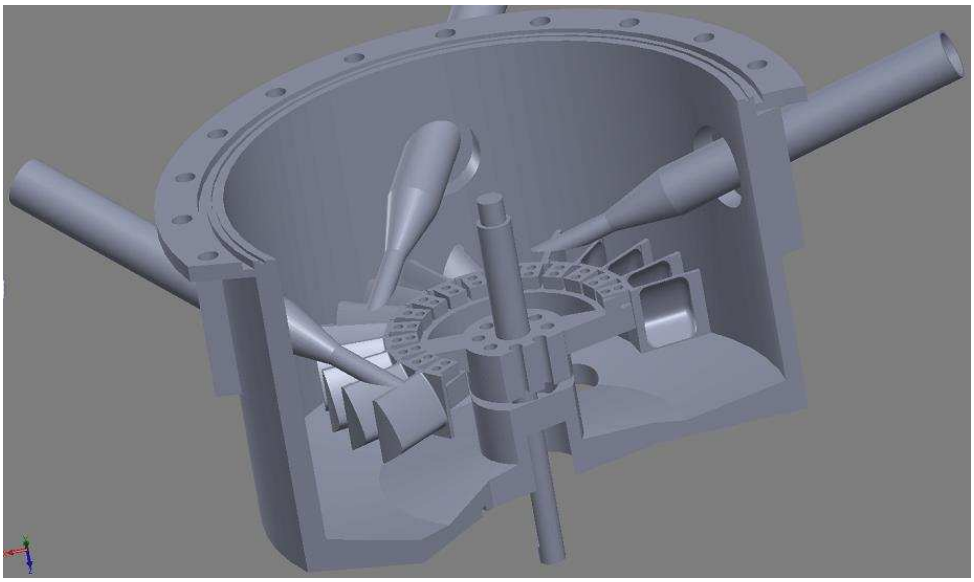

Figure 9: A section view of the enclosure of the turbine.

In Figure 9, three out of the five injectors are visible. It is visible that the injector outlets are tangent to the runner in order to limit the two-phase flow dispersion. The coupling between the buckets and the wheel hub is designed to have the material of the wheel hub bear the shear stress resulting from the moment generated by the two-phase jet injection. The screws that hold the buckets in their place would only have a fixing function and they would be subject to minimal shear stress. The whole structure is also analyzed mechanically; that analysis includes static stress, fatigue stress, and critical frequencies.

4. CONCLUSION

A two-phase Turgo turbine wheel is designed. The friction losses inside the bucket are not high; the two-phase flow only loses 17% of its energy in the bucket due to friction and turbulences. The aerodynamic drag losses amount to only 4% of the power retrieved from the two-phase jet due to the small radius of the runner. The study presented in this article shows the feasibility of using an impulse turbine as a two-phase expander to generate electricity and

increase the refrigeration power of refrigeration systems. The next step in this study would be to build the turbine and to test it to verify the accuracy of this study.

NOMENCLATURE

F	force	N
v	velocity	m/s
ṁ	mass flow rate	kg/s
P	power	W
z	empirical factor	(–)
x	bucket active length	m
b	bucket height	m
ω	angular velocity	rad/s
R	total runner radius	m

Subscript

r	relative between the two-phase jet and the bucket

REFERENCES

Cleary, V., Bowen, P., Witlox, H., 2007, Flashing liquid jets and two-phase droplet dispersion I. Experiments for derivation of droplet atomization correlations", *Journal of Hazardous Materials*, Volume 142, pages 786-796.

Cox, S., 2010, *Losing our cool: Uncomfortable truths about our air-conditioned world (and finding new ways to get through the summer)*, New York: New Press, 272 p.

Diab, Y., Ville, F., Velex, P., 2004, Windage loss in High speed gears – preliminary experimental and theoretical results, *Journal of mechanical design*, vol. 126, no 5, p. 903-908

Polanco, G., Holdø, A.E., Munday, G., 2010, General review of flashing jet studies, *Journal of Hazardous Materials*, Volume 273, pages 2-18.

Yun, S., Lin, Z., 2013, *Control of surge in centrifugal compressors by active magnetic bearings theory and implementation*, Springer, London, 296 p.